Dual-wedge scanning confocal reflectance microscope

William C. Warger II* and Charles A. DiMarzio

Department of Electrical and Computer Engineering, The Bernard M. Gordon Center for Subsurface Sensing and Imaging Systems (Gordon-CenSSIS), Northeastern University, 440 Dana Building, 360 Huntington Avenue, Boston, Massachusetts 02115, USA
**Corresponding author: wwarger@ece.neu.edu*

Received April 10, 2007; revised May 30, 2007; accepted June 1, 2007;
posted June 8, 2007 (Doc. ID 81964); published July 23, 2007

A confocal reflectance microscope has been developed that incorporates a dual-wedge scanner to reduce the size of the device relative to current raster scanning instruments. The scanner is implemented with two prisms that are rotated about the optical axis. Spiral and rosette scans are performed by rotating the prisms in the same or opposite directions, respectively. Experimental measurements show an on-axis lateral resolution of 1.6 μm and optical sectioning of 4.7 μm, which compares with a diffraction-limited resolution of 0.8 and 1.9 μm, respectively. © 2007 Optical Society of America

OCIS codes: 110.0180, 120.3890, 120.4570, 170.1790, 180.1790, 180.5810.

Current point-scanning microscopes generally use a raster scan, which is uniform throughout the field-of-view. However, this standard scan requires an opto-electromechanical configuration that is bulky and difficult to reduce to a handheld device. In this Letter, we discuss the implementation of a dual-wedge scanner as an alternative method to scan the focused spot within a confocal reflectance microscope. This scanner uses two prisms within a compact package to provide a circular two-dimensional scan that is capable of high speeds with a nonuniform pixel density, but requires a detailed mapping algorithm to determine the exact location of the spot. The use of two prisms to scan a laser beam was first described by Rosell in 1960 as a prism scanner [1]. Since then, the scanner has been utilized in various applications under a variety of names that include the rotating prism scanner for optical tracking in guidance systems [2], the dual-wedge scanner for laser radar [3], the Risley prism scanner [4], the double-prism scanner for testing the performance of intersatellite laser communications [5], and the paired-angle rotation scanner for an OCT scanning probe [6].

The concept of the scanner is shown in Fig. 1. A prism with wedge angle α is oriented such that the second surface is normal to the incident collimated laser source and with an angular position θ_1 about the optical axis, where the angular position is measured from the apex of the prism. The incident laser beam is deviated by the vector $\vec{v}_1$ in the sample plane in Fig. 1(a), and the beam scans the dotted circle as the prism is rotated about the optical axis ($\theta_1=0$ to 2π). When an identical prism is placed in the path such that the angular positions of the prisms are the same ($\theta_1=\theta_2$) and the flat surfaces are parallel and facing each other, the beam is deviated by the vector sum $\vec{v}_1+\vec{v}_2$ in Fig. 1(b). If the first prism is held stationary at $\theta_1=0$ and the second prism is rotated about the optical axis, a circle with a radius of $|\vec{v}_2|$ will be scanned about the endpoint of $\vec{v}_1$ in Fig. 1(c). When the prisms are rotated in the same direction and at the same speed ($\omega_1=\omega_2=\omega$) over time t, the angular positions of prism 1 and prism 2 are $\theta_1=\omega t$ and $\theta_2=\omega t+\Delta\theta$, respectively, where $\Delta\theta$ is the angular offset of the two prism apexes, and the beam scans a circle with a radius dependent on $\Delta\theta$. If the prisms rotate in the same direction, but at different speeds ($\omega_1\neq\omega_2$), the angular relationship between the two apexes will change with time and a spiral scan will be produced, similar to the pattern shown in Fig. 2(a). When the prisms are rotated in opposite directions and at the same speed, the angular positions of prism 1 and prism 2 are $\theta_1=\omega t$ and $\theta_2=-\omega t+\Delta\theta$, respectively, and the beam scans a line at an angle $\Delta\theta$. If the prisms rotate in opposite directions, but at different speeds, a rosette scan will be produced, similar to the pattern shown in Fig. 2(b). This description de-

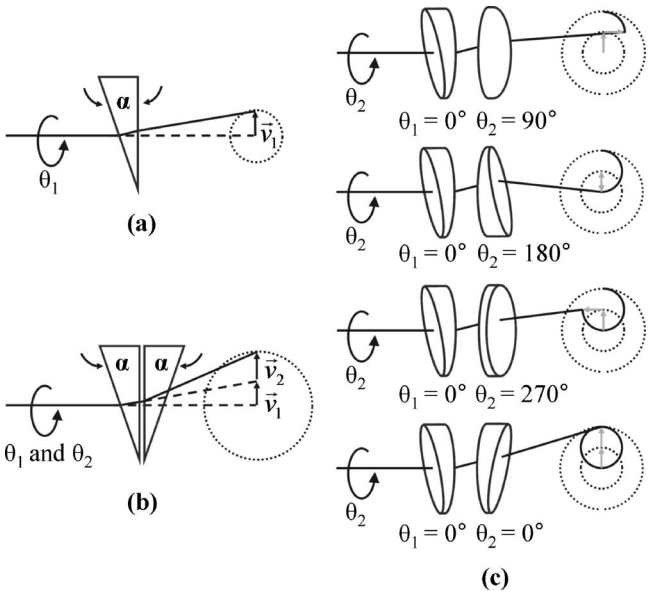

Fig. 1. Scanning concept with prisms of wedge angle α and rotation angles θ_1 and θ_2 about the optical axis. (a) A single prism deviates the beam by the vector $\vec{v}_1$, and (b) two prisms deviate the beam by the vector sum $\vec{v}_1+\vec{v}_2$. (c) A circle is scanned about the deviation from the first prism when the first prism is stationary and the second prism is rotated about the optical axis.

0146-9592/07/152140-3/$15.00

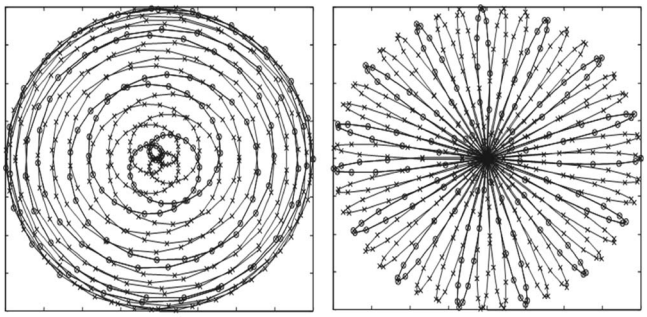

(a) (b)

Fig. 2. Scan patterns produced for (a) co-rotation and (b) counterrotation of the prisms at different speeds.

tails the two most general scan patterns that can be produced, the spiral and rosette scans, but other scan patterns can be generated by changing the relative rotation speeds between the prisms and/or the angles of the prisms [2,4]. However, it is important to note that if two prisms with different wedge angles are used, a circular region with a radius of $||\vec{v}_2|-|\vec{v}_1||$ will not be scanned within the center of the image.

A ray tracing analysis of the two prisms has been performed that calculates the refraction vector [3]:

$$\vec{V}_{j+1} = \frac{n_j}{n_{j+1}}\vec{V}_j + \left[\sqrt{1-\left(\frac{n_j}{n_{j+1}}\right)^2(1-(\vec{V}_j\cdot\vec{N}_j)^2)} - \frac{n_j}{n_{j+1}}\vec{V}_j\cdot\vec{N}_j\right]\vec{N}, \quad (1)$$

where at surface j, $\vec{V}_j$ is a unit vector parallel to the incident beam, $\vec{V}_{j+1}$ is parallel to the refracted beam, $\vec{N}$ is normal to the surface, and n_j is the index of refraction of medium j. When the exact unit vectors are known, a precise analysis of the scan pattern can be completed that includes errors caused by prism tilt, angle disparity between the prisms, misalignment of the incident laser beam, and errors in the registration of the rotation angles. It is possible to correct some of these errors by creating two separate images of a known target. A pixel p is visited twice during a complete scan of the sample, once by the vector sum $p=\vec{v}_1+\vec{v}_2$ and again by the vector sum $p=\vec{v}_2+\vec{v}_1$, where the vectors correspond to the deviation of the beam from the first and second prisms, respectively. Thus, two images can be created by separating the data points into two groups with the test:

$$S = \sin(\theta_1 - \theta_2), \quad (2)$$

within the mapping algorithm. The first image is constructed with data points that correspond to a positive result of Eq. (2), and the second image is created with data points having a negative result. Each of the alignment errors can be adjusted individually by comparing these two images. This method has removed the distortion from each of the images, but a rotation still exists between them, so in this Letter we use one of the two images created with Eq. (2).

We have fabricated a proof-of-principle instrument shown in Fig. 3 that is similar to a standard confocal

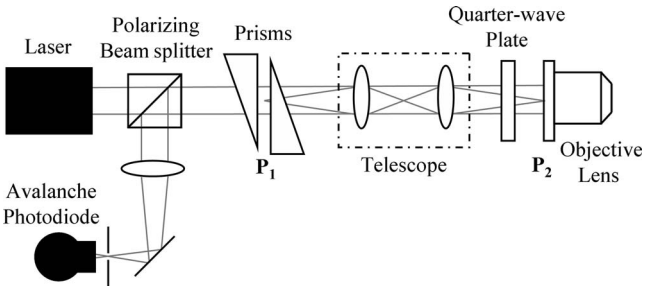

Fig. 3. Optical layout of a confocal reflectance microscope with a dual-wedge scanner.

reflectance microscope with a dual-wedge scanner replacing the raster scanner. The optical path begins at the 830 nm linearly polarized laser diode with a 4.5 mm beam diameter and passes through the polarizing beam splitter with P-polarization. The P-polarized light continues through the dual-wedge scanner and a 2× relay telescope that places the scanner P_1 conjugate to the pupil of the objective lens P_2. The scanner houses 1-inch diameter, 11° prisms ($\alpha=11°$) within two aluminum cylinders, each within a pair of ball bearings and a timing belt pulley. Two timing belts couple identical pulleys on the shafts of the motors and the prism housings to ensure a one-to-one ratio between the prism and the motor rotations. The prism housings are positioned such that the two parallel surfaces of the prisms are separated by 5 mm. A Snell's law analysis using a wedge angle of 11° shows that the focal point of the scanner is 200 μm from the midpoint between the two parallel surfaces. The beam passes through a quarter-wave plate, having an axis oriented at 45° relative to the laser polarization, thereby producing circular polarization, which is then focused into the sample by the objective. The backscattered light that is collected within the numerical aperture of the objective passes back through the quarter-wave plate, telescope, and scanner. On the return path, the light has passed through the quarter-wave plate a second time converting the incident P polarization into S, provided the backscattered light retains its state of polarization as it interacts with the sample. The S-polarized light is reflected by the polarizing beam splitter, toward the avalanche photodiode (APD), and is focused by a lens through a pinhole onto the detector. Throughput measurements show a 41% loss of laser power between the laser and the pupil of the objective lens, a 40% loss between the focus of the objective and the pinhole, and a 4% loss within the scanner.

An image is constructed by simultaneously acquiring the angular position of each prism from the two encoders that are attached to the motors, and the output from the APD (i.e., backscattered light that is detected). A look-up table, constructed by modeling the orientation of the prisms and calculating the refraction vector in Eq. (1) through each of the four surfaces, is used in conjunction with the angular positions to place the intensity value in the correct pixel location. Quantization errors, caused by the discrete encoder positions, discrete pixel locations, and the

mapping between them, create missing data points within the maximally sampled image space that are replaced with the intensity value of the next nearest pixel post-acquisition. Currently, the two prisms are rotated in opposite directions at 1051 and 41 rpm to create a rosette scan similar to Fig. 2(b), and the encoders have a resolution of 1000 cycles per turn. An image is created by sampling 1 million discrete points at a rate of 30 kHz, which is limited by the rotation speed of the fastest prism, to sample 88% of the 1 mm diameter field-of-view with a frame rate of 33 s.

Resolution measurements for the proof-of-principle device were completed on-axis with a 40×, 0.66 NA infinity corrected, air objective lens (Leica). Lateral resolution measurements were completed with the standard method of analyzing a line of sampled pixels that cross a chrome-on-glass edge. The corresponding intensity values were plotted, the 10–90% edge width was measured, and the measured edge width was multiplied by the pixel size in the sample plane. The experimental lateral resolution is 1.6 μm, which is currently limited by the 2 μm pixel size caused by the effective magnification of the system. This measurement compares with the diffraction-limited resolution of 0.8 μm, calculated by

$$\Delta x = 0.6n\lambda/NA, \tag{3}$$

where λ is the center wavelength of the laser diode, NA is the numerical aperture of the objective lens, and 0.6 is the multiplicative factor for a Gaussian spot having a diameter 1.2 times that of the pupil. The multiplicative factor was determined by taking the Fourier transform of a truncated Gaussian beam with the appropriate fill factor, calculating the ideal 10–90% edge width, and converting to units of λ/NA.

The experimentally measured on-axis optical sectioning of the instrument with a 100 μm pinhole is 4.7 μm. The measurement was completed by translating a silver-coated mirror with a $\lambda/20$ surface flatness axially through the focus of the objective, plotting the normalized reflected signal versus the axial

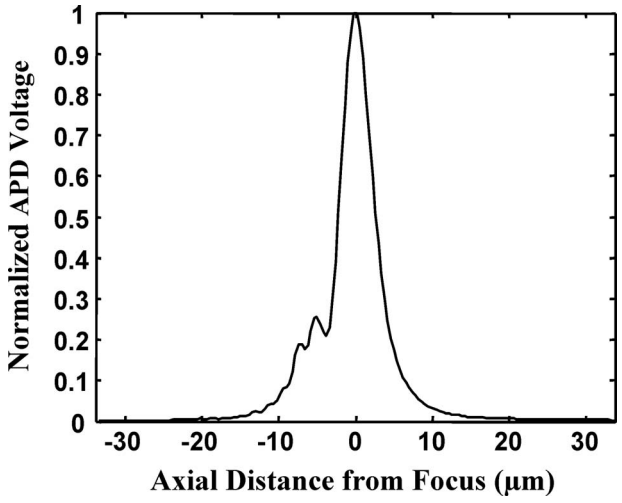

Fig. 4. Optical sectioning measurement of 4.7 μm with a 100 μm pinhole.

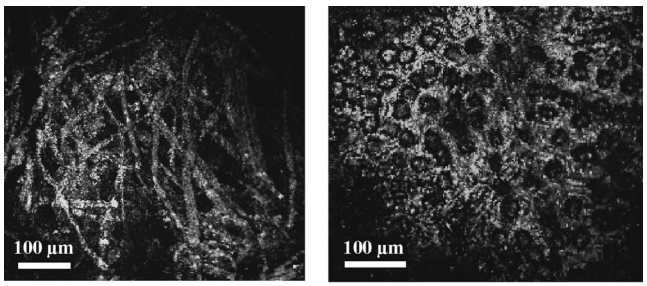

Fig. 5. Images of (a) cellulose fibers within paper and (b) the cellular structure within a plant leaf.

position from focus in Fig. 4, and measuring the FWHM. This measurement compares with the diffraction-limited optical sectioning of 1.9 μm, calculated by [7]

$$\Delta z = 0.95n\lambda/NA^2. \tag{4}$$

Figure 5(a) shows an image of cellulose fibers in paper and Fig. 5(b) shows an image of a plant leaf to demonstrate the sectioning and imaging capabilities of the microscope.

Preliminary measurements and images with the proof-of-principle instrument show promise, but additional work is required to reduce the aberrations and fully characterize the device throughout the field-of-view to compare the performance with raster scanning instruments. In addition, the rotation speed of the prisms must be optimized, and a miniaturized spinning mechanism must be developed along the length of the device to stabilize the scanning system. The timing belt and motor configuration adds a level of uncertainty to the measured rotation angles of the prisms since the encoders are attached to the motors, as opposed to the prism housing, and the timing belt has some elasticity and resonant frequency during rotation. However, the work presented in this Letter shows that a dual-wedge scanner may be incorporated into a confocal reflectance microscope.

The authors thank Stephen Guerrera, Thomas Aites, Christopher Carr, Jeffrey Guizeika, Christopher Marinis, Jamil Abdullah, Megan Rand, Edwin Shirk, and Mohamed Younis for their help designing and fabricating the proof-of-principle instrument. The authors also acknowledge Milind Rajadhyaksha, Daniel Gareau, Peter Dwyer, and Matthew Bouchard. This work has been funded in part by NSF grant EEC-0121931.

References

1. F. A. Rosell, J. Opt. Soc. Am. **50**, 521 (1960).
2. W. L. Wolfe and G. J. Zissis, *The Infrared Handbook* (Office of Naval Research, 1978).
3. C. T. Amirault and C. A. DiMarzio, Appl. Opt. **24**, 1302 (1985).
4. G. F. Marshall, Proc. SPIE **3787**, 74 (1999).
5. A. Li, L. Liu, J. Sun, X. Zhong, D. Xu, Q. Shen, Y. Zhou, Z. Luan, and L. Wang, Proc. SPIE **6304**, 63041R–1 (2006).
6. J. Wu, M. Conry, C. Gu, F. Wang, Z. Yaqoob, and C. Yang, Opt. Lett. **31**, 1265 (2006).
7. T. Wilson *Confocal Microscopy* (Academic, 1990).